Analysis of Nonuniform Nonlinear Distributed Feedback Structures: Generalized Transfer Matrix Method

Stojan Radic, Nicholas George, and Govind P. Agrawal, *Senior Member, IEEE*

***Abstract*— A new method for the analysis of almost-periodic, nonuniform, nonlinear distributed feedback (NLDFB) structures is presented. A grating segmentation technique used for linear DFB devices is combined with the analytic solutions corresponding to a strictly periodic, uniform NLDFB device. The method is demonstrated for tapered, chirped, and phase-shifted structures. New results describing the operation of single- and multiple-phase shifted NLDFB are reported. NLDFB structures with a axially-varying effective Kerr index are also considered.**

I. Introduction

RECENT reports about materials with high third-order nonlinearities [1], [2] have revived interest in nonlinear distributed feedback (NLDFB) structures and, particularly, in their realization as integrated optical devices. The operating characteristics of such structures have been thoroughly investigated by now, both theoretically [3]–[7] and experimentally [8]–[10]. An array of possible applications including optical limiting, switching, multistability and pulse shaping has been proposed [11], [12]. A study of the transient response of these structures [7], [13] has led to the discovery of soliton-like solutions well within the Bragg stop-band, fueling high expectations about their possible role in ultrafast, all-optical switching applications.

Nonuniformities within the NLDFB are either intentionally introduced (designed nonuniformities) or simply represent the artifact of imperfections introduced during the fabrication process. Designed nonuniformities in the form of a grating chirp, taper or phase shift have proved to be quite important for the device performance. It has been demonstrated recently [14] that a combination of taper and chirp can dramatically increase the excitation efficiency of nonlinear waveguide devices. Tapered [15] and segmented [16] designs have been proposed for optimized launching of the gap solitons into a nonlinear periodic structure. Phase-shifted structures feature extremely low switching threshold [17], and represent an important class of nonuniform NLDFB structures. The bistable behavior of a strictly periodic NLDFB device operating in the continuous-wave (CW) regime has been described analytically by Winful in terms of Jacobian elliptic functions [4]. Unfortunately, a general analytic description of nonuniform NLDFB structures is not possible using this approach, leaving us with only numerical techniques.

Considerable effort has been invested in developing the numerical techniques for analyzing nonuniform linear DFB structures [18]–[20]. The latest among these, the transfer-matrix method, [20] divides a nonuniform linear DFB into a set of strictly periodic, uniform segments represented by a corresponding transfer-matrix set. Motivated by the simplicity of this method, we combine the Winful's analytic treatment of the strictly periodic NLDFB and the idea of nonuniform-structure segmentation. In our approach, analytic solutions in the neighboring grating sections are connected by a proper set of the boundary conditions, allowing the field distribution throughout the entire structure to be found. Similar to the transfer-matrix procedure, each grating section is considered to be a two-port element whose transfer function can be exactly calculated. Unlike the case of linear LDFB, where the transfer function solely depends on the input wavelength, the NLDFB transfer characteristic is also dictated by the input magnitude. This approach can be thought as generalization of the linear transfer-matrix method and should be distinguished from existing numerical methods. For this reason, we refer to the proposed method in this paper as the generalized transfer matrix (GTM) method. While a wide class of existing numerical techniques [21]–[24] usually start with the known field distribution for a linear DFB in order to find a self-consistent NLDFB solution by iterative means, our technique can be regarded as a single-sweep, approximate analytic method that demands far less computational effort than other numerical techniques. Furthermore, in the important case of a multiple phase-shifted NLDFB structure, the segmentation along the phase shift locations leads to an exact solution of the problem.

II. Generalized Transfer Matrix Method

Consider a nonuniform NLDFB structure whose index variations are shown in Fig. 1(a) schematically. We assume that optical medium remains uniform in the transverse (x–y) plane, extending in the x and y directions sufficiently far to eliminate consideration of any boundaries. This effectively reduces the problem of finding the field-distribution $E(z)$ to a one-dimensional calculation in the z-direction. The structure nonuniformity in this direction can be partially described by its index of refraction $n = n_L + n^{(2)}|E|^2$, where the linear index n_L varies with z as

$$n_L = n_0 + n_1(z)\cos[2\beta_B(z)z + \Omega(z)]. \quad (1)$$

Manuscript received September 22, 1994. This work was supported in part by the U.S. Army Research Office, the National Science Foundation, and the New York State Science and Technology Foundation.

The authors are with the Institute of Optics, University of Rochester, Rochester, NY 14627 USA.

IEEE Log Number 9411244.

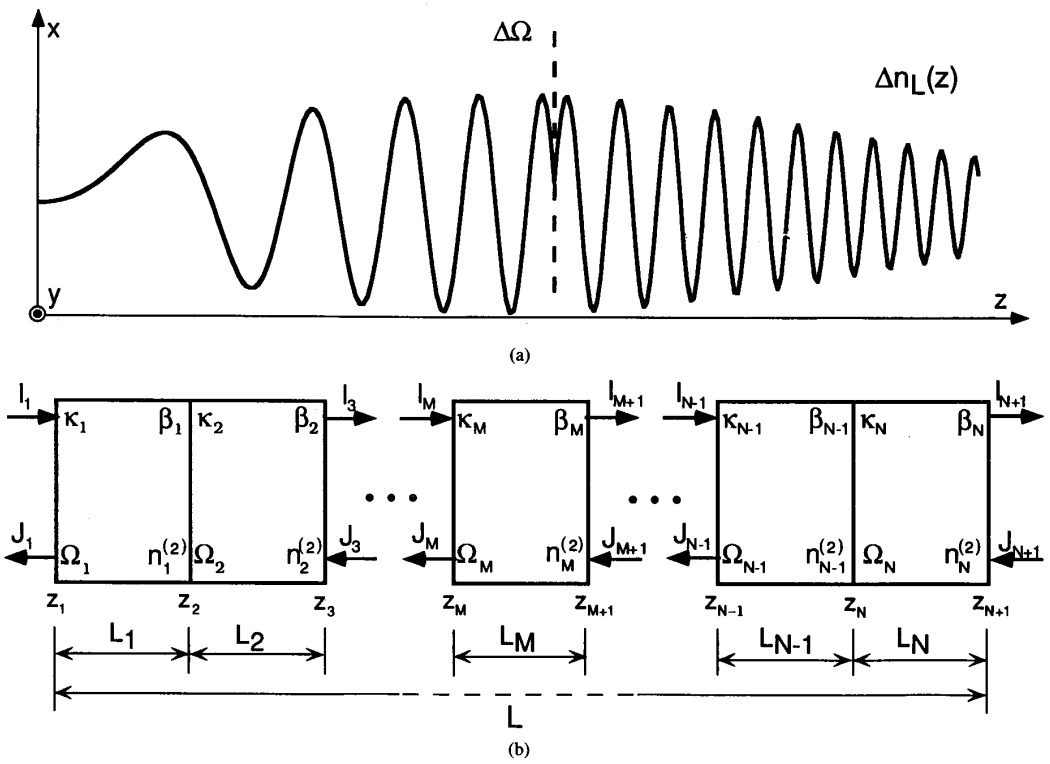

Fig. 1. (a) Schematic index variation in a nonuniform, almost-periodic NLDFB structure with multiple phase shifts $\Delta\Omega$. The structure nonuniformity is represented by the axial variation of the linear refractive index $\Delta n_L(z)$. Additional nonuniformities may include a variation of the Kerr index along the z-axis, $n^{(2)}(z)$. (b) Segmentation of the NLDFB structure from Fig. 1(a) into N strictly-periodic, uniform sections. Each segment is fully characterized by parameters κ_M, β_M, γ_M, Ω_M, and L_M.

Both the index perturbation $n_1(z)$ and the Bragg wave vector $\beta_B(z)$ are slowly-varying functions of z. The Bragg wave vector can be written as

$$\beta_B(z) = \beta_0 + \beta_1(z). \tag{2}$$

The unperturbed Bragg vector β_0 is defined as $\beta_0 = 2\pi/\lambda_0$, and λ_0 is related to the fundamental grating period by $2\Lambda = k\lambda_0$, where k is an integer. The grating phase $\Omega(z)$ remains constant along the structure, except for discrete changes introduced by localized phase shifts $\Delta\Omega(z)$. In the most general case the effective Kerr index can also be allowed to vary along the z-axis as

$$n^{(2)} = n_0^{(2)} + n_1^{(2)}(z). \tag{3}$$

The nonlinear coupled-mode description of the field within the periodic structure implies standard assumptions such as a slowly-varying envelope and moderate coupling strengths [25], [26]. These assumptions remain valid in a wide class of devices (thin-film waveguides, nonlinear multilayer stacks, fiber gratings, etc.), thus allowing us to apply our solutions to a variety of seemingly different problems. The field within the structure is written in its standard form that separates the forward and the backward traveling wave as

$$E(z) = E_+(z)e^{j\beta z} + E_-(z)e^{-j\beta z}, \tag{4}$$

leading to a set of nonlinear coupled mode equations

$$\frac{dE_+}{dz} = i\kappa(z)E_- \exp\left[-2i\Delta\beta(z)z + i\Omega(z)\right] + i\gamma(z) \cdot \left[|E_+|^2 + 2|E_-|^2\right]E_+, \tag{5a}$$

$$\frac{dE_-}{dz} = -i\kappa(z)E_+ \exp\left[2i\Delta\beta(z)z - i\Omega(z)\right] - i\gamma(z) \cdot \left[2|E_-|^2 + |E_+|^2\right]E_-. \tag{5b}$$

The linear coupling parameter $\kappa(z)$ is defined by $\pi n_1(z)/\lambda_0$, and the parameter $\gamma(z)$, responsible for the self- and cross-phase modulation, is defined by $\pi n^{(2)}(z)/\lambda_0$. Frequency detuning from the axially-varying Bragg wave vector is given by $\Delta\beta(z) = \beta - \beta_B(z)$. The analytic solution of (5a) and (5b) is possible only in the case of strictly periodic, uniform or phase-shifted DFB structure characterized by the constant parameters β_B, κ, and $n^{(2)}$. Most of the existing numerical techniques used to treat the general case outlined here are computationally intensive and do not provide the necessary insight into the physics of device operation.

In our approach, we approximate the nonuniform DFB structure by a set of N strictly periodic, uniform segments, as shown in Fig. 1(b). The field distribution within each segment can be calculated analytically, provided that the boundary conditions at one of its interfaces are given. Specifying the field at the end of the structure ($z = L$), one can find the distribution within the Nth segment ($z_N < z \leq L$) and at the

Nth interface ($z = z_N$). Repeating this procedure N times, the front end of the device is reached and the transmittivity of the entire structure is calculated. The coupled mode description of the segmented structure will remain valid as long as the condition

$$L_M \gg 2\pi/\beta_M \tag{6}$$

is satisfied, i.e., as long as the segment length is kept much longer than the period of the DFB grating [20].

Consider now, only the Mth segment, described by a set of a constant parameters (κ_M, β_M, γ_M, Ω_M, L_M). We show that, given the field distribution for $z \geq z_{M+1}$, the field distribution within $z_M \leq z \leq z_{M+1}$ can be calculated exactly, thus allowing for the repetition of the procedure in the $(M-1)$th segment. To solve (5a) and (5b) applied to Mth segment, it is necessary to express the electric field in form separating its magnitude and phase

$$E = |E_\pm(z)| \exp[i\phi_\pm(z)] = A_\pm(z) \exp[i\phi_\pm(z)]. \tag{7}$$

Substitution of (7) into (5a) and (5b) leads to two constants of motion within the Mth segment (Appendix A)

$$G_M = \kappa_M L\sqrt{I(I-T_M)} \cos \Psi_M + [\Delta\beta_M L + 2\eta_M(I - T_m)]I, \tag{8}$$

$$T_M = I - J \tag{9}$$

where

$$\Psi_M(z) = 2\Delta\beta_M z + \phi_+(z) - \phi_-(z) - \Omega_M. \tag{10}$$

The normalized variables $I = A_+^2/A_c^2$ and $J = A_-^2/A_c^2$ are defined as the forward and backward flux, respectively. The critical intensity is defined using the axially-averaged Kerr index

$$A_c^2 = 4\lambda_0/3\pi\overline{n^{(2)}}L; \qquad \overline{n^{(2)}} = \sum_{i=1}^{N} n_i^{(2)}L_i/L. \tag{11}$$

Parameter η_M defines the nonlinearity of the Mth segment: $\eta_M = n_M^{(2)}/\overline{n^{(2)}}$. To give a physical meaning to the critical intensity parameter, consider the case of a 1-cm long GaAs device ($n^{(2)} \sim 1.6 \times 10^{-10}$ esu) operating at $\lambda_0 = 1$ μm. The critical intensity of a such device corresponds to $\sim$1.5 GW/cm^2, a level difficult to reach without inducing thermal damage within the optical medium.

It can be shown that the spatial derivative of the forward flux is related to the segment's phase Ψ_M through the relation, (Appendix A)

$$\frac{dI}{dz} = 2\kappa_M\sqrt{I(I-T_M)} \sin \Psi_M. \tag{12}$$

The importance of the last expression in establishing the proper boundary conditions between two neighboring segments will be seen shortly. The discrete change $\Delta\Omega_M$ of the grating phase introduced at the interface between the two segments introduces the discontinuity in the flux derivative, while maintaining the continuity of the flux itself. The continuity of the flux written in the form

$$I(L_m - \varepsilon)|_{\varepsilon\to 0} = I(L_m + \varepsilon)|_{\varepsilon\to 0}, \tag{13a}$$

$$J(L_m - \varepsilon)|_{\varepsilon\to 0} = J(L_m + \varepsilon)|_{\varepsilon\to 0} \tag{13b}$$

can be combined with (9) to show that the transmitted flux T_M remains conserved not only within each grating section, but also throughout the entire structure

$$T_1 = T_2 = \cdots = T_M = \cdots = T_N = T. \tag{14}$$

Equation (14) is a direct consequence of the zero-gain, lossless model that has been used to describe the response of the optical medium. Finally, elimination of Ψ_M from (8) and (12) allows the construction of the forward flux equation within the Mth segment

$$\left(\frac{L}{2}\frac{dI}{dz}\right)^2 = (\kappa_M L)^2 I(I-T) - \{(\kappa_M L)G_M - [\Delta\beta_M L + 2\eta_M(I-T)I]\}^2 = P(I). \tag{15}$$

Equation (15) can be integrated directly, provided the conserved quantity G_M is given. We now show that such a requirement is equivalent to a knowledge of the intensity distribution $I(z)$ for $z \geq z_{M+1}$. According to (8), the phase $\Psi_{M+1}(z_{M+1})$ within the $(M+1)$th segment can be calculated from

$$\cos \Psi_{M+1}(z_{M+1}) = \{G_{M+1} - [\Delta\beta_{M+1}L + 2\eta_{M+1}(I_{M+1} - T)I_{M+1}]\}/[(I_{M+1} - T)I_{M+1}]^{1/2}. \tag{16}$$

The sign of $\sin \Psi_{M+1}$ recovered from (12), together with (16) provides sufficient information to uniquely define Ψ_{M+1}. Phase within the Mth section is then calculated as follows:

$$\Psi_M(z_{M+1}) = \Psi_{M+1}(z_{M+1}) - \Delta\Omega_M. \tag{17}$$

The constant of motion G_M is calculated by substitution of (17) into (8), thus allowing explicit integration of the equation governing forward flux distribution. The integration can be expressed in the form:

$$\Im = \int_{I(z)}^{I_{M+1}} \frac{dI}{\sqrt{P(I)}} = 2(z_{M+1} - z)/. \tag{18}$$

Evaluation of the integral on the left side of (18) is dependent on the relation among the integration limits $I(z)$, I_{M+1}, and zeros of the polynomial $P(I) = -4\eta_M^2 \prod_{i=1}^{4}(I - I_i^{(0)})$. We focus on the most frequently encountered case in which all zeros $I_i^{(0)}$ ($i = 1, 2, 3, 4$) are real and $I_1^{(0)} \geq I(z)$, $I_{M+1} > I_2^{(0)} > I_3^{(0)} > I_4^{(0)}$, discussing other cases in the Appendix B. In this case the integral $\Im$ is evaluated as

$$\Im = \int_{I(z)}^{I_2^{(0)}} \frac{dI}{\sqrt{P(I)}} + \int_{I_2^{(0)}}^{I_{M+1}} \frac{dI}{\sqrt{P(I)}} = \frac{g}{2\eta_M}\{sn^{-1}[u(I_{M+1}); k] - sn^{-1}[u(I(z)); k]\} \tag{19}$$

where

$$u(I) = [(I_1^{(0)} - I_3^{(0)})(I - I_2^{(0)})/(I_1^{(0)} - I_2^{(0)})(I - I_3^{(0)})]^{1/2} \tag{20}$$

$$g = [(I_1^{(0)} - I_3^{(0)})(I_2^{(0)} - I_4^{(0)})]^{-1} \tag{21}$$

$$k^2 = (I_1^{(0)} - I_2^{(0)})(I_3^{(0)} - I_4^{(0)})g^2. \tag{22}$$

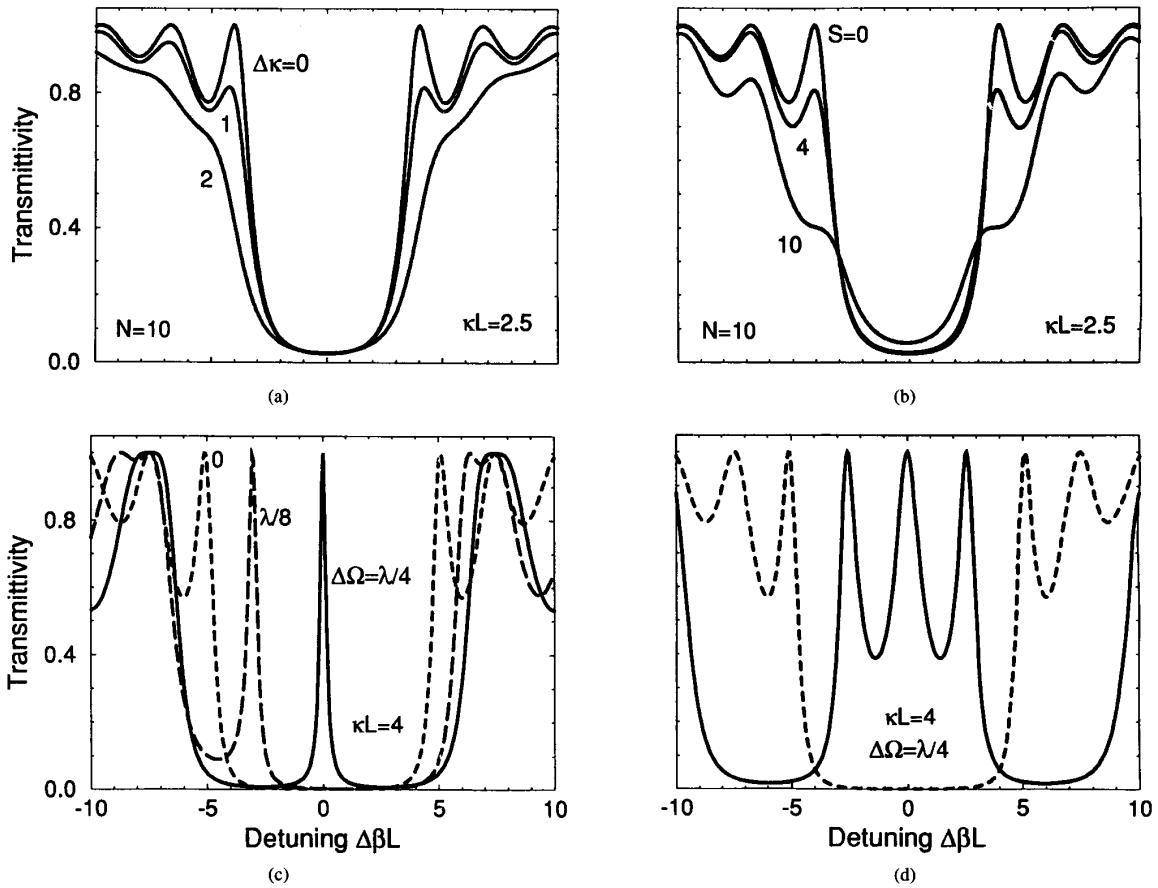

Fig. 2. (a) Low-intensity transmission of a linearly tapered NLDFB with $\kappa L = 2.5$ for three taper parameters: $\Delta\kappa = 0$, 1, and 2. (b) Low-intensity transmittivity of a linearly chirped NLDFB with $\kappa L = 2.5$ for $S = 0$, 4, and 10 and 10-section segmentation is used in the transmission calculation. (c) Low-intensity transmission for uniform (short-dashed curve), $\lambda/8$-shifted (long-dashed curve), and $\lambda/4$-shifted NLDFB (solid curve) NLDFB devices. The phase shift in both cases is located at the center of the structure. (d) Low-intensity transmissivity of a NLDFB device with three equispaced $\lambda/4$ shifts (solid curve). Transmittivity of the uniform NLDFB without phase shifts is indicated by the dashed line. The same intensity parameter $T = 10^{-5}$ is used in plots (a)–(d).

Unfortunately, the inverse elliptic function $sn^{-1}(u; k)$ is multivalued and branches into two distinctive solutions.

$$sn^{-1}(u; k) = F[\sin^{-1}(u); k] = \begin{cases} F(\varphi; k) \\ 2K - F(\pi - \varphi; k) \end{cases} \tag{23}$$

where $F(\varphi; k)$ is the incomplete elliptic integral of the first kind, and $K = F(\pi/2; k)$. The argument φ is defined by both $u = \sin(\varphi + 2\pi n)$ and $u = \sin[-\varphi + (2n + 1)\pi]$. Let us for the moment assume that the proper branch of the function $sn^{-1}(u; k)$ is chosen. Combining the (18) and (19), one can find the explicit formula for the intensity distribution within the Mth segment

$$I(z) = I_3^{(0)} + \frac{I_2^{(0)} - I_3^{(0)}}{1 - \dfrac{I_1^{(0)} - I_2^{(0)}}{I_1^{(0)} - I_3^{(0)}} sn^2(z)} \tag{24}$$

where $sn(z)$ is a symbolic notation for

$$sn(z) = sn\{sn^{-1}[u(I_{M+1}); k] - 4\eta_M(z_{M+1} - z)/gL; k\}. \tag{25}$$

The axial derivative of the intensity distribution is calculated from (24) in the form

$$\frac{dI(z)}{dz} = 2\frac{I(z) - I_3^{(0)}}{\dfrac{I_1^{(0)} - I_3^{(0)}}{I_1^{(0)} - I_2^{(0)}} - sn^2(z)} sn(z)cn(z)\,dn(z). \tag{26}$$

Equation (12) provides an independent mean to calculate this derivative at the interface $z = z_{M+1}$

$$\left(\frac{dI}{dz}\right)_{z=z_{M+1}-\varepsilon} = \frac{(\sin\Psi_M)_{z=z_{M+1}-\varepsilon}}{(\sin\Psi_{M+1})_{z=z_{M+1}+\varepsilon}} \cdot \left(\frac{dI}{dz}\right)_{z=z_{M+1}+\varepsilon}. \tag{27}$$

The calculation of the flux derivative using either of (26) and (27) produces the identical result only if the proper branch of

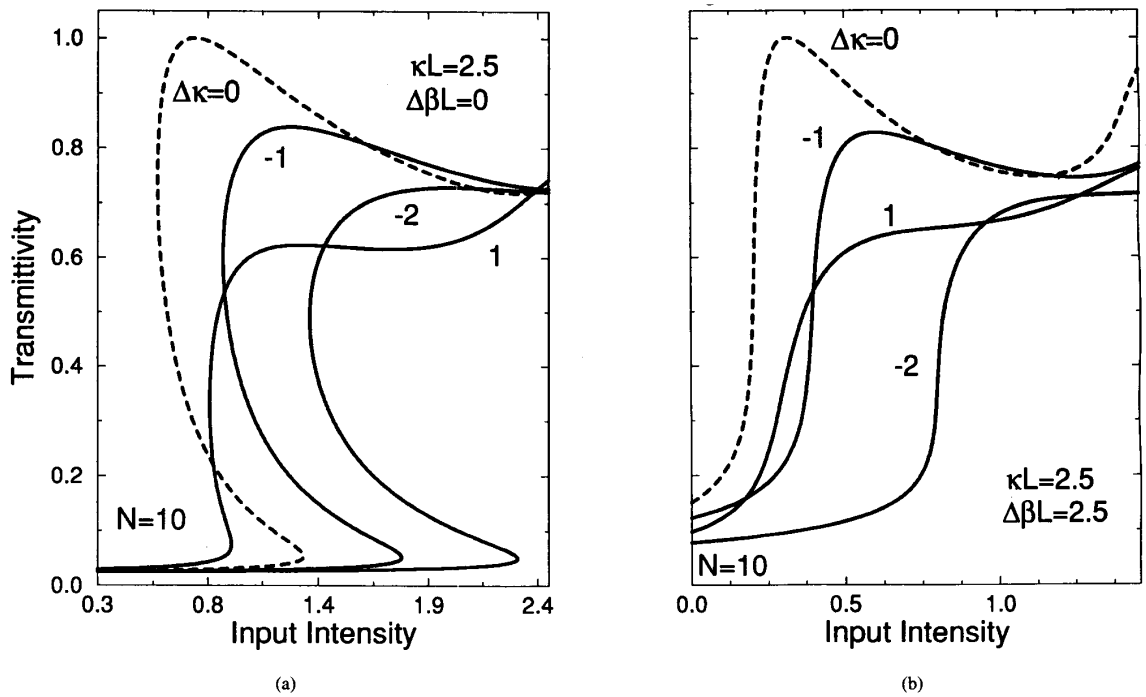

(a) (b)

Fig. 3. (a) Transmission characteristics of linearly tapered NLDFB with $\kappa L = 2.5$, tuned to the center of Bragg stop-band ($\Delta\beta L = 0$) for parameters $\Delta\kappa = -2, -1, 0$, and 1. (b) Transmission characteristics of an identical structure tuned to the edge of the stop-band ($\Delta\beta L = 2.5$).

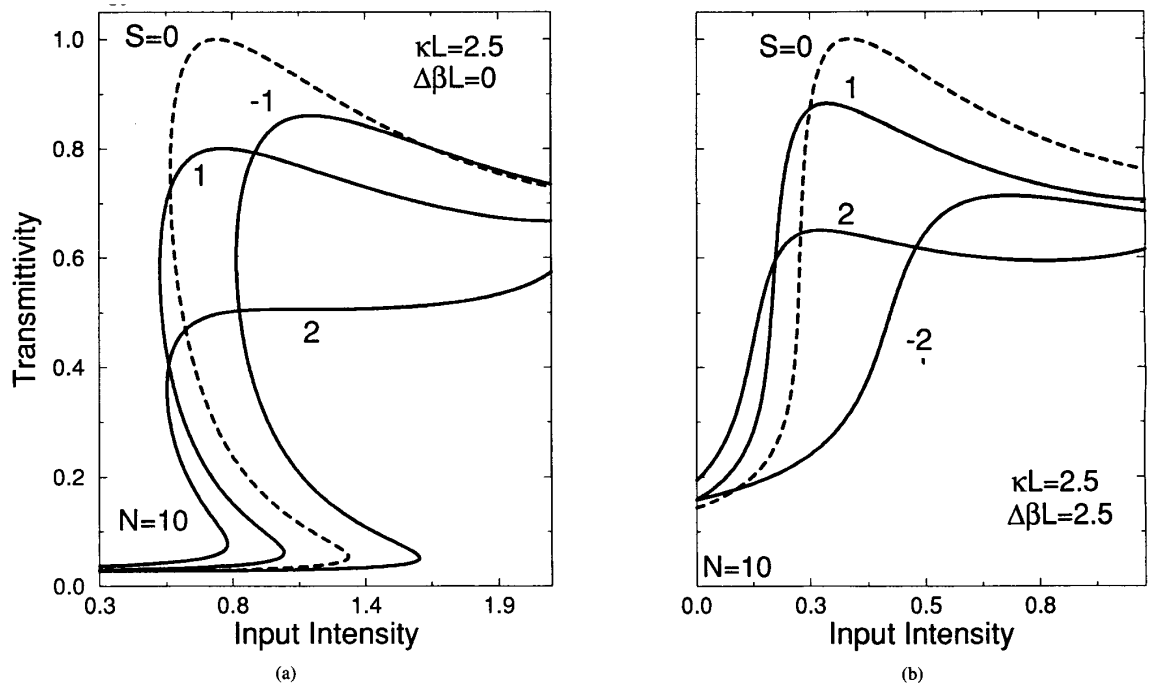

(a) (b)

Fig. 4. (a) Transmission characteristics of linearly chirped NLDFB with $\kappa L = 2.5$, tuned to the center of the stop-band ($\Delta\beta L = 0$) for $S = -1, 0, 1$, and 2. (b) Transmissivity of an identical NLDFB structure tuned to an edge of the stop-band.

the function sn^{-1} is chosen, thus allowing us to find a unique distribution $I(z)$ within the Mth segment.

To summarize, the following procedure should be followed when using the GTM technique.

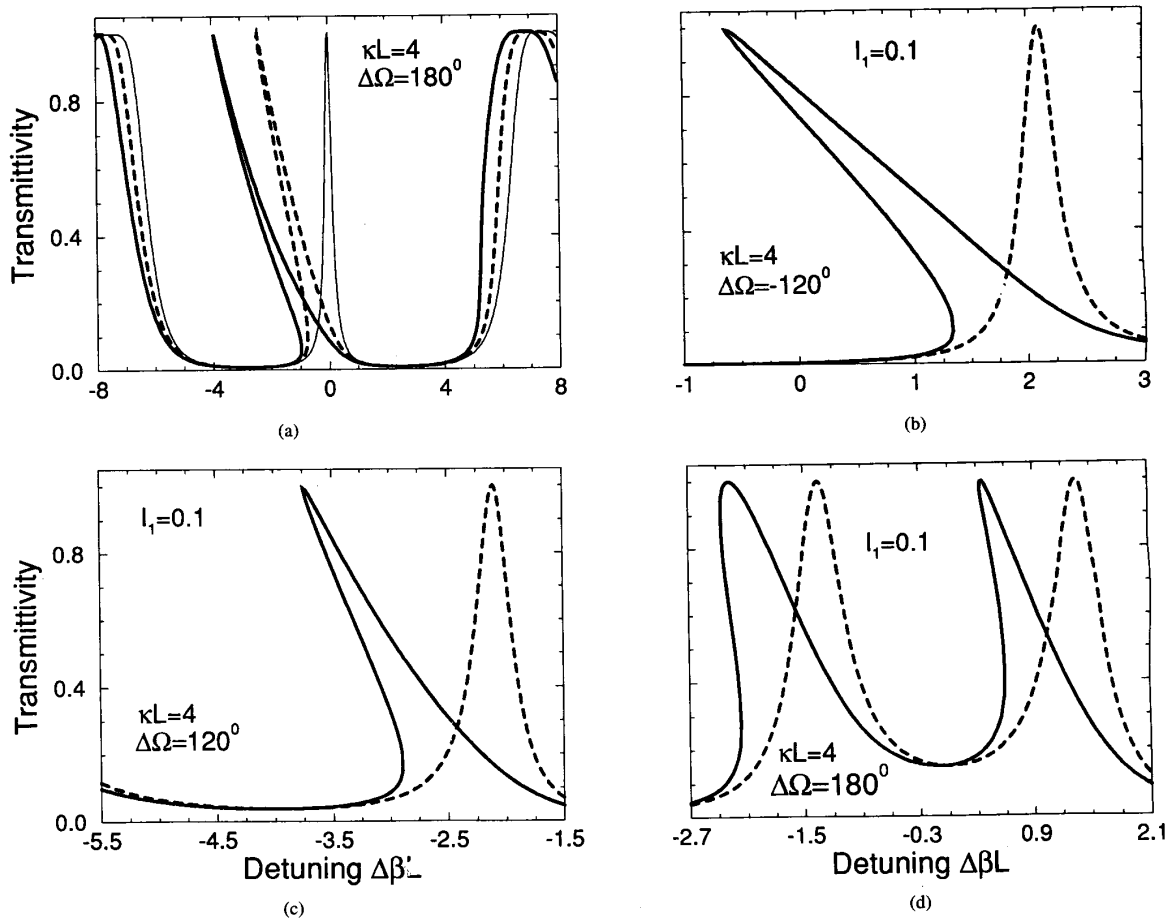

Fig. 5. (a) Transmittivity of $\lambda/4$-shifted structure with $\kappa L = 4$ for three different input intensities: $I_1 = 10^{-5}$ (thin solid curve), 0.1 (dashed curve), and 0.2 (heavy solid curve). (b) Transmittivity of NLDFB with $\kappa L = 4$ and $\Delta\Omega = -120°$ (located at its center) for $I_1 = 10^{-5}$ (dashed line) and $I_1 = 0.1$ (solid line). (c) Transmittivity of NLDFB with $\kappa L = 4$ and $\Delta\Omega = 120°$ for $I_1 = 10^{-5}$ (dashed line) and $I_1 = 0.1$ (solid line). (d) Transmission of NLDFB with $\kappa L = 4$ and two identical phase shifts of 180° located at $z = 0.35\ L$ and $z = 0.65\ L$. Dashed and solid line correspond to $I_1 = 10^{-5}$ and $I_1 = 0.1$, respectively.

1) Divide the structure into a proper number of segments in order to satisfy both the sectional length condition (6) and to achieve convergence of the solution.
2) Provide the boundary condition at the output of the device ($z = L$) first. It is convenient to use a nonreflective condition at the interface $z = L$ simply by setting the value of transmitted flux $T = I(L)$. Reflective interfaces can be considered with a straightforward modification.
3) Use (24) to calculate the forward flux distribution within each uniform section of the grating and its axial derivative to connect solutions in the neighboring segments.
4) Once the front end of the device is reached, the transmitted flux parameter T can be changed and the above procedure repeated. This is equivalent to generating an ordered triplets (I_1, T, $\Delta\beta$). For each output parameter T, the one and only one input value I_1 is found for a given frequency detuning. Due to a multistable behavior of NLDFB, the opposite does not have to be true. The calculation of the device transmittivity requires fixed input I_1 across the entire frequency detuning region and is easily performed by sorting the triplets with a given I_1.

III. Results and Discussion

We now illustrate the GTM technique by analyzing tapered, chirped and phase-shifted NLDFB structures. The method is also demonstrated for NLDFB devices with an axially-varying Kerr index. Before considering each case in detail, we first need to test the GTM performance in the low-intensity operating regime. In this limit, the NLDFB transfer characteristics approaches that of the linear DFB structure. Since they are well known, [18]–[20] they can serve as a reference for the GTM algorithm. Fig. 2(a)–(d) shows the transmittivities of the linearly tapered, linearly chirped, single- and multiple-phase shifted NLDFB device operating at $T = 5 \times 10^{-5}$. Each plot agrees remarkably well with the linear DFB calculation, exhibiting deviations of less than 1% from the well-known analytic results for the chosen value of $N = 10$.

Linearly Tapered NLDFB: Linear taper of the form

$$\kappa(z) = \kappa_0[1 + \Delta\kappa(z - L/2)/L] \tag{28}$$

is introduced into strictly periodic, uniform NLDFB, maintaining the average coupling parameter $\kappa_0 = 2.5$. The influence

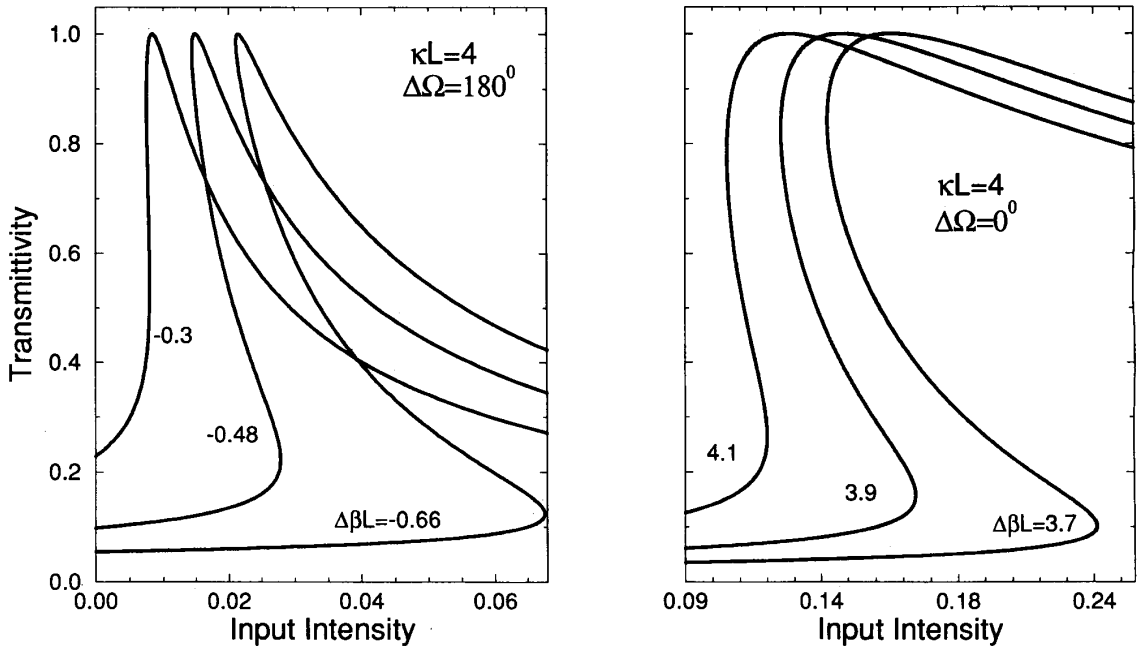

Fig. 6. (a) Transmission characteristics of $\lambda/4$-shifted NLDFB with $\kappa L = 4$ for three detuning parameters: $\Delta\beta L = -0.66, -0.48$, and -0.3. (b) Transmission characteristic of the edge-tuned, uniform NLDFB device with $\kappa L = 4$ for three detuning parameters: $\Delta\beta L = 3.7$, 3.9, and 4.1.

of different taper forms on the device operation has been studied in detail before [23], so we limit the discussion to a GTM analysis of the linear taper only. Transmittivity of the NLDFB in the low-intensity level is shown in Fig. 2(a) for the parameters $\Delta\kappa = 0$, 1, and 2, exhibiting characteristic sidelobe disappearance [17], [18] with the increasing $\Delta\kappa$. The solution converges very quickly, with only 10 DFB segments used to approximate continuously varying taper function $\kappa(z)$. The zero-detuning transmission characteristics are shown in Fig. 3(a) for parameters $\Delta\kappa = -2, -1, 0, 1$, confirming the disappearance of the hysteresis for the positive detuning, as reported earlier [23]. The properties of the device tuned near an edge of the Bragg stop-band are of particular interest, because of the lower switching intensities expected in this region. Fig. 3(b) shows the influence of the linear taper when the edge-tuning at $\Delta\beta L = 2.5$ is chosen. In the absence of a taper ($\Delta\kappa = 0$), almost nonexisting hysteresis still allows up-switching at $I_1 \sim 0.18$, as compared to the zero-detuning value of $I_1 \sim 1.3$. Negative taper considerably increases I_1 while decreasing the total throughput efficiency at the same time. Positive taper further deteriorates the NLDFB performance by leveling the up-switching slope.

Linearly Chirped NLDFB: The periodicity of the uniform NLDFB is changed by introducing the linear chirp

$$\Delta\beta = \beta_o + S(z - L/2)/L. \tag{29}$$

Fig. 2(b) shows the well-known effects of the chirp in the low-intensity limit ($T = 5 \times 10^{-5}$), when the device can be approximated by LDFB. Smoothing of the sidelobes and the transmission increase near the $\Delta\beta L = 0$ are in agreement with the previous linear calculation [19], [20]. The transmission characteristics of the device tuned at the center of the stop-band are plotted in Fig. 4(a) for the parameters $S = -1$, 0, 1, and 2. As reported earlier [24], negative values of the chirp parameter S increase the up-switching intensity and decrease the overall efficiency of the device. A positive chirp in addition decreases the width of the transmission hysteresis. The zero-detuning performance of the NLDFB is compared to that of the edge-tuned device in Fig. 4(b). It is evident that both positive and negative values of the chirp severely affect operation of the device in both tuning regimes by lowering transmission efficiency and decreasing the hysteresis width.

Phase-Shifted NLDFB: Since their first introduction, phase-shifted LDFB structures have been extensively used [27]–[30], most notably for design of single-mode semiconductor sources. $\lambda/4$-shifted devices, the best known class of these structures, feature a narrow transmission peak in the middle of the Bragg stopband, offering the possibility of a narrow-band filter design.

In comparison with the phase-shifted LDFB, similar nonlinear structures have received relatively little attention in spite of their exceptional transmission characteristics. The extremely low switching intensities for the $\lambda/4$-shifted NLDFB structure have been reported recently [17]. Fig. 2(c) and (d) shows the transmission of a single and multiple phase-shifted NLDFB in low-intensity limit. The grating is segmented at the phase-shift locations, making the GTM method exact in this case. Fig. 5(a) shows the transmittivity of a $\lambda/4$-shifted NLDFB for different

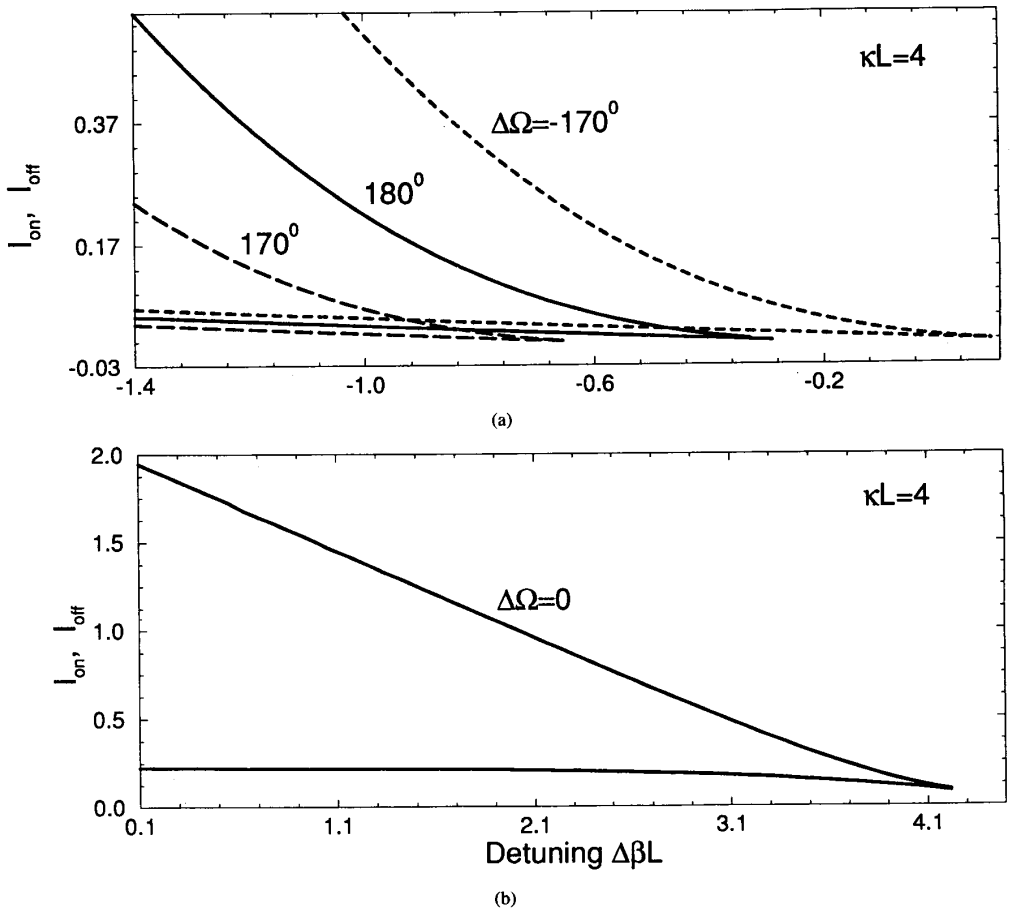

Fig. 7. (a) I_{on}–I_{off} characteristics showing the hysteresis width for a phase-shifted device in cases when $\Delta\Omega$ =170° (long-dashed line), 180° (solid line), and −170° (short-dashed line). Lower horizontal portion of each characteristic represents downswitching intensities (I_{off}), while upper, curved portion represents upswitching intensities (I_{on}). (b) The I_{on}–I_{off} characteristic corresponding to the otherwise identical, uniform NLDFB plotted separately because a different intensity scale.

values of the input intensity: $I_1 = 10^{-5}$, 0.1, and 1. A very large frequency shift is exhibited by the central transmission peak, while edges of the stop-band ($\Delta\beta L \approx \pm 5$) remain almost fixed. Transmission characteristics of the structure are plotted in Fig. 6(a) for detunings of $\Delta\beta L = -0.3$, -0.48, and -0.66, showing the signs of the hysteresis at input intensities as low as $I_1 \sim 0.015$. This should be contrasted with the uniform ($\Delta\Omega = 0$), edge-tuned device which starts exhibiting hysteresis at about $I_1 \sim 0.12$. Fig. 7 emphasizes this point by plotting the hysteresis position and width for phase-shifted (Fig. 7(a)) and uniform (Fig. 7(b)) structures. By varying phase-shift values $\Delta\Omega$, the position, and the width of the hysteresis can be dramatically changed: a decrease of only 10° will translate hysteresis into the negative direction for $\Delta\beta L = 0.5$, lowering the switching intensities at the same time.

The reason behind the low switching intensities required for the $\lambda/4$-shifted NLDFB is apparent from the intradevice intensity distribution, shown in Fig. 8(a). In the low-intensity limit ($I_1 < 0.02$), the intensity at the device center $z = L/2$ is almost an order of magnitude higher than the input intensity I_1. Such a high center intensity modifies the local refractive index at the phase-shifting location, effectively increasing the initial phase retardation of 180°. The net effect is that a $\lambda/4$-shifted NLDFB structure looses its transparency at $\Delta\beta L = 0$ even for moderate input levels. The edge-tuned device (Fig. 8(b)) initially shows a similar type of behavior (as the input intensity is increased from the low linear limit, the mid-device intensity builds up) but never reaches the levels comparable to those of the $\lambda/4$-shifted device. In addition, the peak-intensity position does not remain localized in the center, but slowly shifts toward the end of the structure.

Fig. 5(b) and (c) show the importance of the chosen phase shift $\Delta\Omega$ for the device operation. A phase shift of $\Delta\Omega = -120°$ opens the transmission peak at $\Delta\beta L \sim 2$ (Fig. 5(b)). For a moderate input intensity of $I_1 = 0.1$, this peak is shifted to $\Delta\beta L \sim -0.75$, a distance of almost three detuning units. If a phase shift with the opposite sign is chosen ($\Delta\Omega = 120°$), the transmission peak at $\Delta\beta L \sim -2$ is opened (Fig. 5(c)), and for the same input intensity level, is shifted only for 1.5 detuning units ($\Delta\beta L \sim -3.6$),—one half of the previous

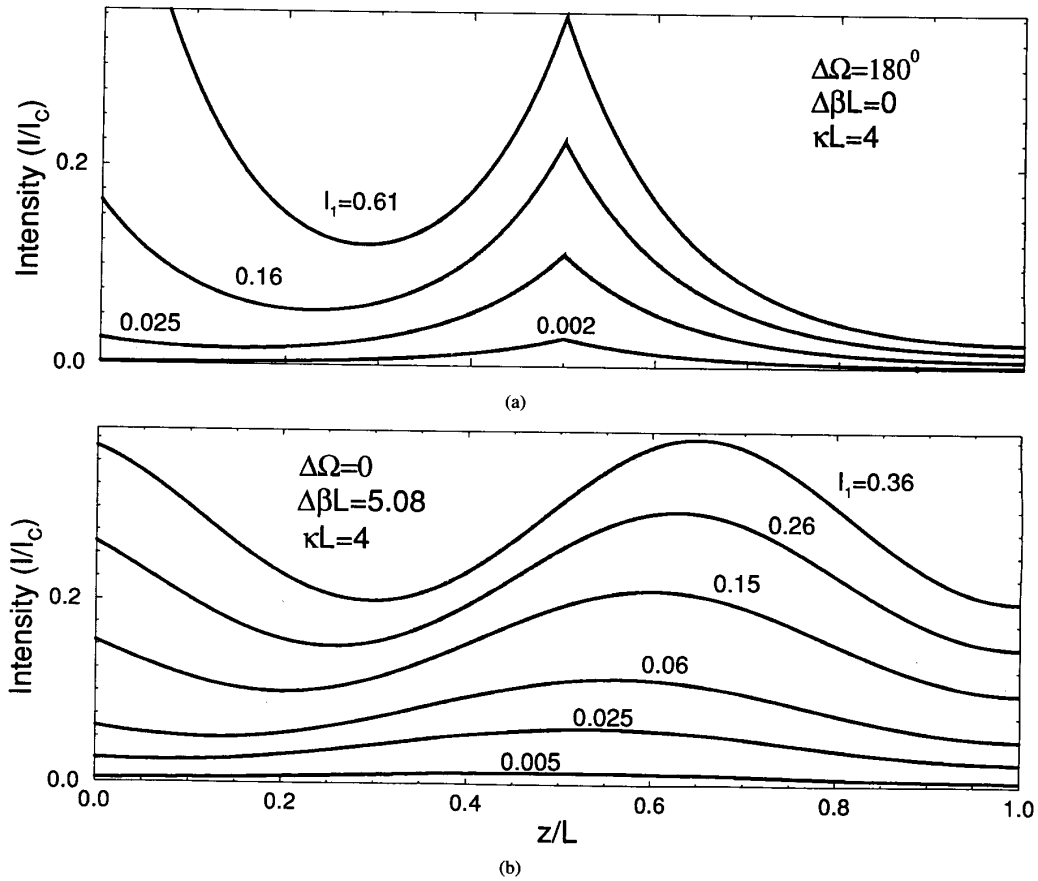

Fig. 8. (a) Axial distribution of the intradevice intensity $I(z)$ for the case of $\lambda/4$-shifted NLDFB with $\kappa L = 4$. The structure is tuned to the center of the stop-band ($\Delta\beta L = 0$). (b) The axial distribution of the intradevice intensity for the case of edge-tuned, uniform NLDFB with $\kappa L = 4$.

value. If the objective is to design a wide hysteresis device operating at low intensity and tuned by varying the input wavelength, a choice of $\Delta\Omega = -120°$ is clearly the superior one. However, if switching efficiency is more important, the choice of the $\Delta\Omega = 120°$ device may be a better one.

The case of multiple phase shifts is shown in Fig. 5(d). The structure has two identical $\lambda/4$ phase shifts located at $z = 0.35\ L$ and $z = 0.65\ L$. As the Input intensity is increased to $I_1 = 0.1$, both transmission peaks are shifted by approximately one detuning unit. However, the widths of the transmission peaks have considerably changed, introducing differences between their up-switching efficiencies.

NLDFB with Axially Varying Kerr Index: Until now, we have assumed that effective Kerr index remains constant by setting $\eta_M = n_M^{(2)}/\overline{n^{(2)}} = 1$. The GTM method permits this parameter to be varied along the z-axis, allowing the analysis of nonuniformly doped devices with the z-dependent effective Kerr index. To make a meaningful comparison with the uniform NLDFB structure, we choose the following form for the parameter $\eta(\xi = z/L)$

$$\eta(\xi) = 2 - \{1 - \exp[-(2\xi - 1)^2/D^2]\}/ [1 - D\sqrt{\pi}\,\mathrm{erf}\,(D^{-1})/2]. \quad (30)$$

The Gaussian in (30) has the $1/e$-width of D and is centered at $\xi = 1/2$. Appearance of the error function in this expression is the result of the requirement that average parameter $\overline{\eta}$ remains unity as in the case of uniform NLDFB. The maximum of the $\eta(\xi)$ is reached for $\xi = 1/2$ and is equal 2; i.e., the maximum value of the local Kerr index never exceeds twice the value of the Kerr index considered in previous examples. We set the width of the Gaussian to be $D = L/2$ in all cases.

Fig. 9(a) shows the transmittivity of a uniform NLDFB width $\kappa L = 2$ and input intensity of $I_1 = 1$. The structure becomes fully transparent for this input level at $\Delta\beta L = 0$. The transmittivity of an identical NLDFB except for a Gaussian Kerr index is plotted in Fig. 9(b) for the same input intensity. The stronger local Kerr index allows for a bigger stop-band shift in case of the NLDFB, thus, moving the 100% transmission peak further into negative detuning region.

The $\lambda/4$-shifted structure with the Gaussian nonlinear index given by (30) and $I_1 = 1$ is considered in Fig. 10. The transmission peak corresponding to nonuniform NLDFB is shifted further than that of the uniform Kerr index device. The stronger Kerr index at $z = L/2$ requires much lower intensities to alter the 180° phase-retardation of the NLDFB,

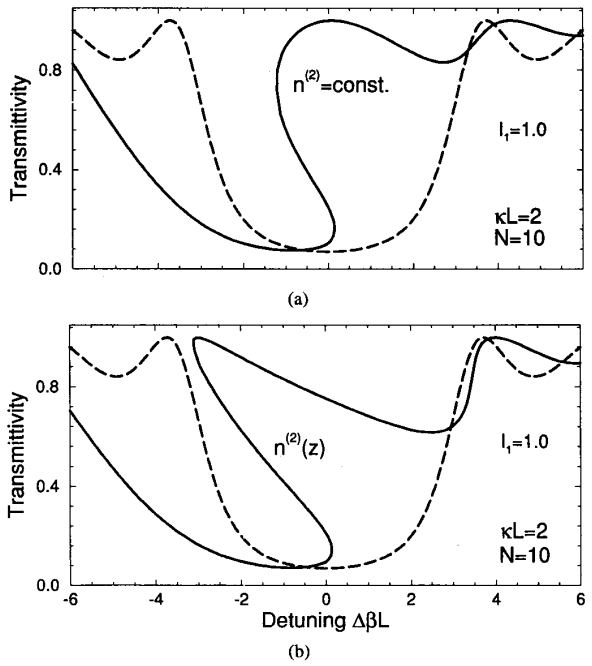

Fig. 9. (a) Transmission of the uniform NLDFB with $\kappa L = 2$ and input intensity $I_1 = 1.0$ corresponding to a full transparency at the center of the stop-band ($\Delta\beta L = 0$). (b) Transmission of the NLDFB with $\kappa L = 2$ and Gaussian variation of the effective Kerr index, as described in text. The input intensity is kept at the same level: $I_1 = 1.0$.

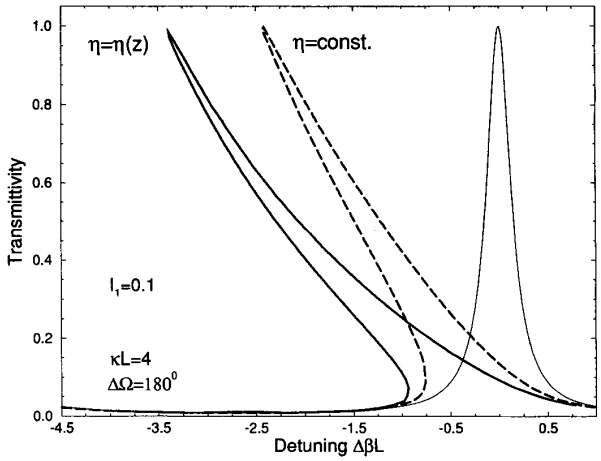

Fig. 10. Transmission of the $\lambda/4$-shifted NLDFB with $\kappa L = 4$ and uniform Kerr index, for the input intensity of $I_1 = 10^{-5}$ (thin solid curve) and $I_1 = 0.1$ (dashed curve). Transmission of the otherwise identical $\lambda/4$-shifted structure having a nonuniform Kerr index is indicated by heavy solid line for the same input intensity $I_1 = 0.1$.

effectively making the nonuniform device more "sensitive" to input changes.

IV. Conclusion

We have presented novel generalized transfer matrix method for analysis of nonuniform, almost-periodic NLDFB structures. The new approach takes advantage of the exact solutions corresponding to a strictly-periodic, uniform NLDFB and the grating segmentation technique known from the linear DFB structure analysis. The GTM method is demonstrated for the commonly used tapered and chirped nonuniform NLDFB devices, showing complete agreement with the previously reported results. Particular attention is devoted to phase-shifted NLDFB structures, treated exactly by the GTM technique. In addition, calculations for the NLDFB with an axially-varying effective Kerr index are presented. The results show that switching device can be made more sensitive by this technique.

It is difficult to overemphasize the importance of the nonuniform NLDFB structure design, particularly in integrated and waveguide optics applications. We feel that proposed technique offers the means for a quick and straightforward characterization of these structures, regardless of their complexity or operating regime.

Appendix A
Constants of Motion in Uniform, Strictly-Periodic Nonlinear DFB Structure

In order to find the conserved quantities within the uniform NLDFB, the counterpropagating field components are written in a form that separates their magnitude and phase

$$E_{\pm}(z) = |E_{\pm}(z)|e^{i\phi_{\pm}(z)} = A_{\pm}(z)e^{i\phi_{\pm}(z)}. \quad \text{(A1)}$$

After substitution of (A1) into (5a), (5b) and separation of imaginary and real parts, we obtain

$$\frac{dA_+}{dz} = \kappa A_- \sin\Psi \quad \text{(A2)}$$

$$\frac{dA_-}{dz} = \kappa A_+ \sin\Psi \quad \text{(A3)}$$

$$A_+\frac{d\phi_+}{dz} = \kappa A_- \cos\Psi + \gamma(|A_+|^2 + 2|A_-|^2)A_+ \quad \text{(A4)}$$

$$A_-\frac{d\phi_-}{dz} = \kappa A_+ \cos\Psi + \gamma(|A_-|^2 + 2|A_+|^2)A_- \quad \text{(A5)}$$

where Ψ is defined by (10). Elimination of Ψ from (A2) and (A3) results in a first constant of motion, transmitted flux

$$A_T^2 = A_+^2(z) - A_-^2(z). \quad \text{(A6)}$$

By taking the z-derivative of (A7) and using (A2)–(A5), one can easily prove that $dG/dz = 0$, showing that

$$G = \kappa L\sqrt{I(I-T)}\cos\Psi + [\Delta\beta L + 2\eta(I-T)]I \quad \text{(A7)}$$

represents the second constant of motion for the uniform NLDFB. For more detailed proof that does not assume previous knowledge of the form of (A7), see [31].

Appendix B
Direct Integration of the Forward Flux Equation

The forward flux equation (15), can be regarded as the energy equation of a classical particle [31], [32] moving in the quartic potential $V = -P(I)$. The zeros of the polynomial $P(I)$ then represent boundaries of the confinement region for the classical particle defined by nonnegative value I. Three different cases are generally encountered.

1) All four zeros of the polynomial $P(I)$ are real and $I_1^{(0)} \geq I_{M+1}$, $I(z) > I_2^{(0)} > I_3^{(0)} > I_4^{(0)}$. This is the case discussed in text by relations (19)–(24).

2) Zeros form a real and complex conjugate pair, and $I_1^{(0)} \geq I_{M+1}$, $I(z) > I_2^{(0)}$, $I_3^{(0)} = I_4^{(0)*}$. In this case, using the (18), one can show that forward flux has the following form [33], [34]:

$$I(z) = I_2^{(0)} + \frac{I_1^{(0)} - I_2^{(0)}}{1 + \dfrac{|I_1^{(0)} - I_3^{(0)}|}{|I_2^{(0)} - I_3^{(0)}|} \dfrac{1 + cn(z)}{1 - cn(z)}}. \quad \text{(B1)}$$

The symbolic meaning of $cn(z)$ is similar to that of (25).

3) All four zeros are real, and $I_1^{(0)} > I_2^{(0)} > I_3^{(0)} \geq I_{M+1}$, $I(z) > I_4^{(0)}$. The forward flux expression in this case can be found [33], [34] to have a form similar to a expression in case 1):

$$I(z) = I_1^{(0)} + \frac{I_1^{(0)} - I_4^{(0)}}{1 - \dfrac{I_3^{(0)} - I_4^{(0)}}{I_3^{(0)} - I_1^{(0)}} sn^2(z)}. \quad \text{(B2)}$$

REFERENCES

[1] H. W. H. Lee, R. S. Hughes, J. E. Davis, C. F. McConaghy, A. V. Hamza, and M. Balooch, "Feasibility of fullerene thin films for high-speed all-optical switching," in *Proc. CLEO, Opt. Soc. Am.*, Washington, DC, 1994, p. 59.

[2] D. Neher, W. E. Torruellas, K. B. Rochford, M. B. Marques, R. Zanoni, G. Assanto, and G. I. Stegeman, "Nonlinear optical probes of conjugated polymers," *Synth. Metals*, vol. 49, pp. 21–35, 1992.

[3] M. Okuda and K. Onaka, "Bistability of optical resonator with distributed Bragg-reflectors by using Kerr effect," *Jpn. J. Appl. Phys.*, vol. 16, pp. 769–773, 1977.

[4] H. G. Winful, J. H. Marburger, and E. Garmire, "Theory of bistability in nonlinear distributed feedback structures," *Appl. Phys. Lett.*, vol. 35, pp. 379–381, 1979.

[5] W. Chen and D. L. Mills, "Optical response of nonlinear multilayer structures: Bilayers and superlattices," *Phys. Rev.*, vol. B36, pp. 6269–6278, 1987.

[6] C. Martijn de Sterke and J. E. Sipe, "Extension and generalizations of an envelope-function approach for the electrodynamics of nonlinear periodic structures," *Phys. Rev.*, vol. A39, pp. 5163–5178, 1989.

[7] D. N. Christodoulides and R. I. Joseph, "Slow Bragg solitons in nonlinear periodic structures," *Phys. Rev. Lett.*, vol. 62, pp. 1746–1749, 1989.

[8] J. He, M. Cada, M. A. Dupertuis, D. Martin, F. M. Genoud, C. Rolland, and A. J. Spring Thorpe, "All-optical bistable switching and signal regeneration in a semiconductor layered distributed-feedback/Fabry–Perot structure," *Appl. Phys. Lett.*, vol. 63, pp. 866–868, 1992.

[9] N. D. Sankey, D. F. Prelewitz, and T. G. Brown, "All-optical switching in a nonlinear periodic-waveguide structure," *Appl. Phys. Lett.*, vol. 60, pp. 1427–1429, 1992.

[10] C. J. Herbert and M. S. Malcuit, "Optical bistability in nonlinear periodic structures," *Opt. Lett.*, vol. 18, pp. 1783–85, 1993.

[11] H. G. Winful and G. I. Stegeman, "Applications of nonlinear periodic structures in guided wave optics," in *Proc. SPIE*, vol. 517, 1984, pp. 214-218.

[12] J. E. Ehrlich, G. Assanto, and G. I. Stegeman, "Nonlinear guided-wave grating phenomena," in *Proc. SPIE*, vol. 1280, 1990, pp. 136–149.

[13] C. Martijn de Sterke and J. E. Sipe, "Switching dynamics of finite periodic nonlinear media: A numerical study," *Phys. Rev. A*, vol. 42, pp. 2858–2869, 1990.

[14] G. Li, J. A. Tobin, and D. D. Denton,"Excitation of nonlinear guided waves in Kerr-type media using chirped and tapered gratings," *J. Opt. Soc. Am. B*, vol. 83, pp. 2290–2297, 1993.

[15] C. Martijn de Sterke and J. E. Sipe, "Launching of gap solitons in nonuniform gratings," *Opt. Lett.*, vol. 18, pp. 269–271, 1993.

[16] H. A. Haus, "Matching of distributed-feedback structures," *Opt. Lett.*, vol. 15, pp. 1134–1136, 1992.

[17] S. Radic, N. George, and G. P. Agrawal, "Theory of low-threshold optical switching in nonlinear, phase-shifted, periodic structures," *J. Opt. Soc. Am. B,*, vol. 12, Apr. 1995.

[18] M. Matsuhara, K. O. Hill, and A. Watanabe, "Optical-waveguide filters: Synthesis," *J. Opt. Soc. Am.*, vol. 65, pp. 804–808, 1975.

[19] H. Kogelnik, "Filter response of nonuniform almost-periodic structures," *Bell. Syst. Tech. J.*, vol. 55, pp. 109–126, 1976.

[20] M. Yamada and K. Sakuda, "Analysis of almost-periodic distributed feedback slab waveguides via a fundamental matrix approach," *Appl. Opt.*, vol. 26, pp. 3474–3478, 1987.

[21] M. Koshiba, *Opt. Waveguide Analysis.* New York: McGraw-Hill, 1990.

[22] J. He and M. Cada, "Combined distributed feedback and Fabry–Perot structures with a phase matching layer for optical bistable devices," *Appl. Phys. Lett.*, vol. 61, pp. 2150–2152, 1992.

[23] G. Assanto, R. Zanoni, and G. I. Stegeman, "Effects of taper in nonlinear distributed feedback gratings," *J. Mod. Opt.*, vol. 35, pp. 871–883, 1988.

[24] G. Assanto and R. Zanoni, "Almost-periodic nonlinear distributed feedback gratings," *Ott. Fis.*, vol. 23, pp. 89–101, 1990.

[25] H. Kogelnik and C. V. Shank, "Coupled-wave theory of distributed feedback lasers," *J. Appl. Phys.*, vol. 43, pp. 2327–2335, 1972.

[26] A. Yariv, "Coupled-mode theory for guided-wave optics," *IEEE J. Quantum Electron.*, vol. QE-9, pp. 919–933, 1973.

[27] H. A. Haus and C. V. Shank, "Antisymmetric taper of distributed feedback lasers," *IEEE J. Quantum Electron.*, vol. QE-12, pp. 532–539, 1976.

[28] G. P. Agrawal and A. H. Bobeck, "Modeling of distributed feedback semiconductor lasers with axially-varying parameters," *IEEE J. Quantum Electron.*, vol. 24, pp. 2407–2414, 1988.

[29] J. N. Damask and H. A. Haus, "Wavelength-division multiplexing using channel-dropping filters," *J. Lightwave Technol.*, vol. 11, pp. 424–428, 1993.

[30] G. P. Agrawal and S. Radic, "Phase-shifted fiber Bragg gratings and their application for wavelength demultiplexing," *IEEE Photon. Technol. Lett.*, vol. 6, pp. 995–997, 1994.

[31] H. G. Winful, "Optical bistability in periodic structures and in four-wave mixing processes," Ph.D. thesis, Univ. of Southern California, 1980.

[32] L. A. Lugiato and R. Bonifacio, "Mean field theory of optical bistability and resonance fluorescence," *Coherence in Spectroscopy and Modern Physics,* F. T. Arecchi, R. Bonifacio, and M. O. Scully, Eds. New York: Plenum, 1978, p. 85.

[33] P. F. Byrd and M. D. Friedman, *Handbook of Elliptic Integrals for Engineers and Scientists.* New York: Springer-Verlag, 1971.

[34] M. Abramowitz and I. A. Stegun, *Handbook of Mathematical Functions.* New York: Dover, 1965.

Stojan Radic, photograph and biography not available at the time of publication.

Nicholas George, photograph and biography not available at the time of publication.

Govind P. Agrawal (M'83–SM'86), photograph and biography not available at the time of publication.